Research in Astron. Astrophys. **2012** Vol. **12** No. **4**, 453–464
http://www.raa-journal.org *http://www.iop.org/journals/raa*

***R**esearch in*
***A**stronomy and*
***A**strophysics*

Relative flux calibration for the Guoshoujing Telescope (LAMOST) *

Yi-Han Song[1,2,3], A-Li Luo[1,2,⋆], Georges Comte[1,4], Zhong-Rui Bai[1,2], Jian-Nan Zhang[1,2], Wei Du[1,2,3], Hao-Tong Zhang[1,2], Jian-Jun Chen[1,2], Fang Zuo[1,2] and Yong-Heng Zhao[1,2]

[1] National Astronomical Observatories, Chinese Academy of Sciences, Beijing 100012, China; *lal@lamost.org; lal@nao.cas.cn*
[2] Key Laboratory of Optical Astronomy, National Astronomical Observatories, Chinese Academy of Sciences, Beijing 100012, China;
[3] Graduate University of Chinese Academy of Sciences, Beijing 100049, China;
[4] Observatoire Astronomique Marseille-Provence and Laboratoire d'Astrophysique de Marseille, F-13388 Marseille Cedex, France

Received 2011 April 21; accepted 2011 May 12

Abstract This paper presents a relative flux calibration method for the Guoshoujing Telescope (LAMOST), which may be applied to connect a blue spectrum to a red spectrum to build the whole spectrum across the total wavelength range (3700 $\sim$ 9000 Å). In each spectrograph, we estimate the effective temperatures of selected stars using a grid of spectral line indices in the blue spectral range and a comparison with stellar atmosphere models. For each spectrograph, stars of types A and F are selected as pseudo-standard stars, and the theoretical spectra are used to calibrate both the blue (3700 $\sim$ 5900 Å) and red spectrograph arms (5700 $\sim$ 9000 Å). Then the spectral response function for these pseudo-standard stars could be used to correct the raw spectra provided by the other fibers of the spectrograph, after a fiber efficiency function has been derived from twilight flat-field exposures. A key problem in this method is the fitting of a pseudo stellar continuum, so we also give a detailed description of this step. The method is tested by comparing a small sample of LAMOST spectra calibrated in this way on stars also observed by the Sloan Digital Sky Survey. The result shows that the $T_{\rm eff}$ estimation and relative flux calibration method are adequate.

Key words: techniques: spectroscopic — calibration: methods:data analysis

1 INTRODUCTION

The Large Sky Area Multi-Object Fibre Spectroscopic Telescope (LAMOST, now called the Guoshoujing Telescope) is a 4-meter reflecting Schmidt telescope with a 5 degree field of view and 4000 fibers in the focal plane (Su et al. 1998). In the commissioning phase since 2009, the test observations identified many problems of data reduction that need to be solved.

∗ Supported by the National Natural Science Foundation of China.

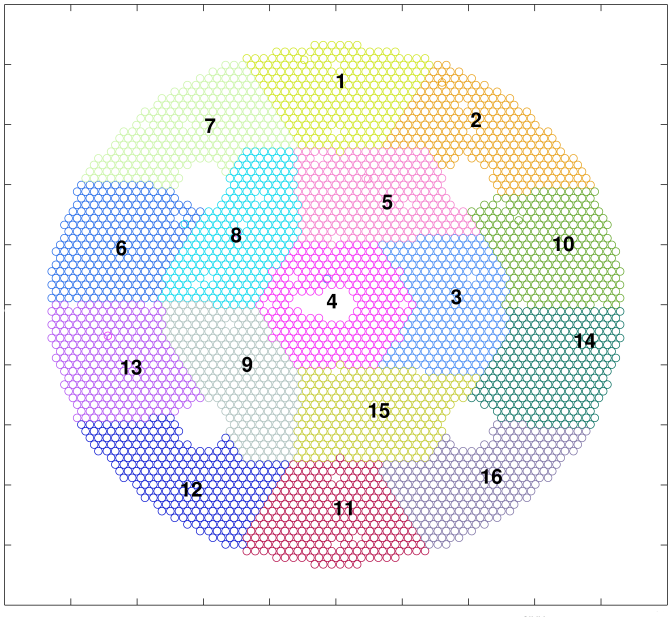

Fig. 1 Focal plane of LAMOST; 16 sub areas are connected with 16 spectrographs through fibers. The numbers on the plane are the spectrograph identification numbers (*color online*).

The final products of the LAMOST telescope should be flux calibrated spectra, with each spectrum being the relationship between the radiation flux of a celestial body and the wavelength of the radiation. This relationship can be expressed as $f(\lambda)$, whose physical unit is $\mathrm{erg\ cm^{-2}\ s^{-1}\ \AA}$. Because there is still no network of photometric standard stars for LAMOST, this instrument can now only provide relative fluxes, i.e. $\log\ f(\lambda) + C$, where C is a constant. This paper proposes a robust method to derive such a relationship between relative flux and wavelength for each observed object.

The observed spectra can be expressed as

$$f_{\mathrm{obs}}(\lambda) = f(\lambda) \otimes I_i(\lambda) \otimes A(\lambda)\,, \tag{1}$$

where $f_{\mathrm{obs}}(\lambda)$ is the observed flux of a celestial body, $f(\lambda)$ is the physical flux we want to recover, $I(\lambda)$ is the instrument spectral response and $A(\lambda)$ is Earth's atmosphere spectral response. The flux calibration process is the restoration of $f(\lambda)$ from $f_{\mathrm{obs}}(\lambda)$. Even for relative flux calibration, there are still limitations, because they are directly related to the properties of LAMOST's focal plane.

The focal plane of LAMOST has a 1.75 m diameter covering a 20 square degree field of view. There are 4000 fibers mounted on it, with a minimal separation between two objects of $5.5'$. Thus the whole set of fibers covers the entire focal plane except for five holes, where four guiding CCD cameras and one Shack-Hartmann sensor are mounted. Each subset of 250 neighboring fibers is grouped into a bundle that feeds light into one of 16 spectrographs, see Figure 1. Hence, each spectrograph covers slightly more than one degree of field. Sun & Hu (1997) mentioned the need to consider the effects of atmospheric dispersion for large sky area multi-object fiber telescopes. These authors computed the effects of dispersion at the Xinglong Station. The result shows that there is no obvious effect of dispersion at the zenith point, and the effect increases along with decreasing altitude. It means that the $A(\lambda)$ is a constant in Equation (1).

In the Sloan Digital Sky Survey (hereafter SDSS), F8 stars in each field are selected as standard spectrophotometric stars, and these stars could also be used as standard stars for LAMOST. However, there may not be enough standard stars for a given LAMOST field, either because of the large sky area of this field, or because the area surveyed by LAMOST is outside that surveyed by SDSS. In this paper, we propose a method that yields an estimation of the effective temperature of stars, not cataloged as standards, on non-calibrated spectra. Using the Kurucz model[1] atmospheres with close values of the estimated temperature, we can regard those stars as pseudo-standard stars.

In Section 2 we discuss the precondition and assumption for the LAMOST relative flux calibration work. The method that estimates the $T_{\rm eff}$ of the target from a non-calibrated spectrum is detailed in Section 3, where we use Kurucz model spectra to generate a grid of Lick spectral indices. The $T_{\rm eff}$ of the target spectrum is estimated by comparing its Lick indices to that of the Kurucz model spectra. We also check the accuracy of the method and analyze the systematic error by comparing the $T_{\rm eff}$ computed by us with those derived by the SEGUE Stellar Parameter Pipeline (hereafter SSPP) of SDSS on a large sample of stars. In Section 4 we discuss the process of calibration that leads to the derivation of the spectral response function of the LAMOST spectrographs. We estimate the range of temperatures under which the stars are most suitable as pseudo-standards. A robust method to fit the pseudo-continuum is also presented in Section 4. In Section 5, we give some preliminary results of the method, and compare spectra obtained with LAMOST and SDSS on a small common sample of objects.

2 PRECONDITION AND ASSUMPTION

According to the computation in Sun & Hu (1997) the effect of dispersion is very small across one degree of sky area around the zenith. For testing the present method of relative flux calibration, we shall make the assumption that the objects are all near the zenith, and that the atmospheric dispersion is consistent across the field of one spectrograph. It means that $A(\lambda)$ is a constant in Equation (1). In future observations, a sky model will be computed and integrated into the processing of the data to allow for the effects of atmospheric dispersion.

Because of LAMOST's extremely large focal plane, across which uniformity of artificial illumination is exceedingly difficult to achieve, a flat field cannot be provided by a laboratory source. Therefore, we use twilight illumination for flat fielding. The twilight frames show that the efficiency variance of the fibers belonging to the same spectrograph is small.

Figure 2 shows, as an example, the efficiency variance of fibers of the 1st, 13th, and 16th spectrographs. Figure 2 displays the variance of the flux collected by the 250 fibers in a twilight exposure, sampled at intervals of 100 Å, before and after a flat-fielding procedure has been applied. This procedure consists of selecting the 30 most efficient fibers, coadding their spectra, and slightly smoothing the resulting spectrum to make a "masterflat." Then all 250 individual spectra are divided by this masterflat, producing individual spectral efficiency distributions. These are subsequently smoothed by a two-pass broad median filter to remove high frequency noise (most of which is due to the numerous faint absorption lines in the solar spectrum of twilight) and keep the low and medium spatial frequency components. As a check, the raw twilight individual fiber spectra are divided by the corresponding resulting spectral fiber efficiencies, and the variance of the resulting flux is again measured at 100 Å intervals. Figure 2 shows that the raw variance is around 10% to 20% but drops down to a maximum of 2% after application of the procedure. This variance is indeed the error of the $I_i(\lambda)$ in Equation (1). Hence we may assume that $I_i(\lambda)$ is uniform for one spectrograph. This is a precondition for the flux calibration work.

With the assumption and the precondition, we are able to calibrate the spectra by using standard star(s) in the same spectrograph. Because there is no photometric telescope associated with

[1] *http://kurucz.harvard.edu*

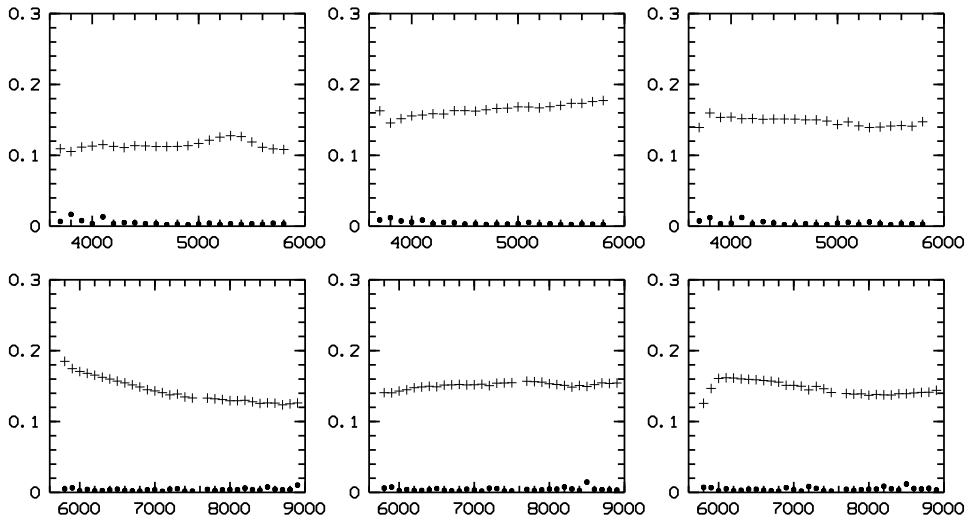

Fig. 2 Variance distribution of the flux collected by the 250 fibers of a given spectrograph in a twilight exposure. Wavelength in Å is on the abscissa. On the ordinate, the standard deviation of the fiber flux, normalized to the local mean of this flux at the selected wavelength, is plotted at 100 Å intervals. The upper curve (*pluses*) is the observed variance before flat-fielding, and the lower curve (*dots*) is the distribution of the residual variance after the flat fielding procedure described in the text has been applied. Top row: blue arms of spectrographs 1 (*left*), 13 (*center*), and 16 (*right*); bottom row: corresponding red arms. The 7600 Å point is not plotted; the data there are not significant because of the very deep atmospheric A band absorption.

LAMOST, we shall calibrate the flux of LAMOST spectra in the relative form of $\log(f(\lambda)) + C$ where C is a constant.

3 ESTIMATING THE EFFECTIVE TEMPERATURE OF STARS

3.1 Lick Indices

A spectral index is an estimate of the equivalent width of a spectral feature, measured by taking the ratio of the flux observed in a narrow wavelength band centered on the feature with respect to a local pseudo-continuum defined in adjacent wavebands. Up to now, many sets of spectral indices have been defined, among which the most successful and famous one is the Lick−IDS index system developed since 1985 by a team of astromomers (Burstein et al. 1984; Faber et al. 1985; Burstein et al. 1986; Gorgas et al. 1993; Worthey et al. 1994; Trager et al. 1998). The Lick−IDS system consists of 25 atomic and molecular absorptions defined on spectra obtained with the Lick low resolution spectrograph using the Image Dissector Scanner (IDS; Robinson & Wampler 1972). It is widely applied to study the star formation histories of galaxies and to determine the stellar atmospheric parameters of stars.

We have studied the effect of continuum aberrance on Lick indices. First of all, we extracted the shapes of continua of a number of uncalibrated LAMOST stellar spectra to build a library of continuum shapes from real stars. Second, we multiplied a newly aquired stellar spectrum with each shape from the continuum shape library to form a spectrum with a modified local continuum. This simulation alters the local continuum. Third, Lick indices were respectively computed for spectra with both a modified and original local continuum. Comparison of the two sets of index values

convinced us that local continuum aberrance has little effect on Lick indices. More details on these simulations will be described in a forthcoming paper (Du W. et al, 2012, in preparation).

Since only the blue arm spectrum is used to estimate $T_{\rm eff}$, the spectral range excludes TiO_1, TiO_2, NaD, Fe5782, and Fe5709 indices in the Lick index definition. The remaining 20 lines include $T_{\rm eff}$ sensitive lines, i.e. Balmer lines, and metallicity sensitive lines. Both Balmer lines and metal lines are used because their equivalent width (EW) values are affected by $T_{\rm eff}$, surface gravity ($\log\ g$), and metallicity ([Fe/H]), avoiding the degeneration of these effects.

3.2 Grid of Line Indices

We have measured 20 blue line indices on 1818 Kurucz theoretical spectra and have built a grid of stellar parameters, with $T_{\rm eff}$ from 3500 K to 10 000 K in steps of 250 K, while [Fe/H] ranges from 0 to –4.0 dex and $\log g$ ranges from 0.0 to 5.0. Because $T_{\rm eff}$ and [Fe/H] are coupled together when estimating the atmospheric stellar parameters, $T_{\rm eff}$ cannot be accurately estimated without metallicity information. Fixing gravity and metallicity allows an easier estimate of $T_{\rm eff}$. With different $\log g$ and [Fe/H], the center of the distribution of the $T_{\rm eff}$ values should be close to the real temperature. Therefore, we have divided the measured theoretical spectra into 77 groups (seven steps in [Fe/H] and 11 steps in $\log g$) so that spectra in the same group have the same gravity and metallicity. Then, we compute the target spectrum's best $T_{\rm eff}$ in each group, and we call it the Best Group $T_{\rm eff}$. We also search for the best $T_{\rm eff}$ from *all* theoretical spectra, and we call it the Best Model $T_{\rm eff}$. To find the best $T_{\rm eff}$ in each case we compare the Lick indices of the target spectrum to the Lick indices of the theoretical spectra. The best $T_{\rm eff}$ is the $T_{\rm eff}$ of the model which is at the smallest distance from the target spectrum in the space of Lick indices.

To get an estimate of the actual $T_{\rm eff}$ of the target, we make three hypotheses. 1. The Best Model $T_{\rm eff}$ is close to the actual $T_{\rm eff}$. 2. The actual gravity and metallicity are in the range of those of the Best Model. 3. The number of our model spectra is large enough. Because gravity and metallicity will affect the estimated temperature, some Best Group $T_{\rm eff}$ will be larger than the actual $T_{\rm eff}$ and also some others may be smaller. The Best Group $T_{\rm eff}$ will cluster around the actual $T_{\rm eff}$. With these three assumptions, we can estimate our target $T_{\rm eff}$ using the following steps: 1. Compute the Best Model $T_{\rm eff}$. 2. Compute 77 Best Group $T_{\rm eff}$. 3. Exclude Best Group $T_{\rm eff}$ which differs by more than 1000 K from the Best Model $T_{\rm eff}$. 4. The average of the remaining Best Group $T_{\rm eff}$ will be the final estimated $T_{\rm eff}$.

3.3 The Accuracy of Temperature Estimation by the Grid

There are many similarities between the LAMOST telescope and the Sloan telescope. They both use fiber technology to provide spectra. The spectral range and resolution of these two instruments are similar . The SDSS spectra have accurate flux calibration and the parameters which are derived from them have been used by many astronomers for years. They are very suitable for testing our method.

To check the accuracy of $T_{\rm eff}$ estimation by our grid method, we have randomly selected 21 571 stellar spectra from SDSS Data Release 8 (DR8). The atmospheric parameters of these stars are extracted from the SDSS DR8 CAS (the most recently updated parameters).

Figure 3 displays the comparison between temperatures from SDSS SSPP (SEGUE Pipeline), on the ordinate, and the values estimated by our method, on the abscissa. The red dashed line represents the 1:1 line. The blue solid line is a linear fit of the principal data cloud. The difference between the two lines carries evidence for a systematic error that can be corrected using

$$T_{\rm eff,grid} = T_{\rm eff,grid,raw} \times 0.7519 + 1578.6\,, \qquad (2)$$

where $T_{\rm eff,grid,raw}$ is the temperature estimated by the Lick grid method, and $T_{\rm eff,grid}$ is the value corrected from the systematic error. After applying the correction, the mean error is $\sigma_T = 205$ K. It is smaller than the step size of our grid.

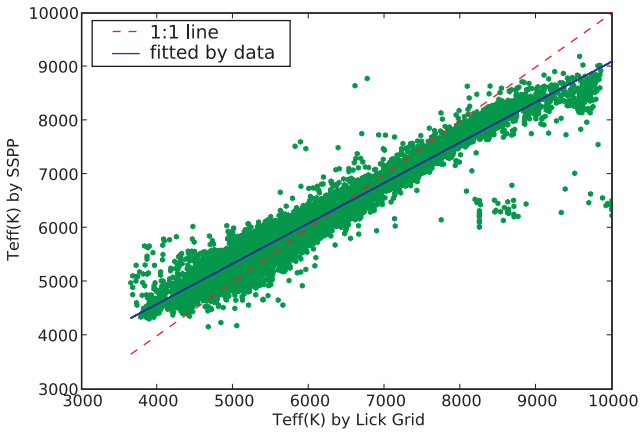

Fig. 3 Effective temperatures derived by our method (x direction) versus those provided by SDSS SSPP (y direction). The points are 21 844 stars from SDSS DR8. The red dashed line is the 1:1 relation (*color online*). The solid line is a linear fit of the data.

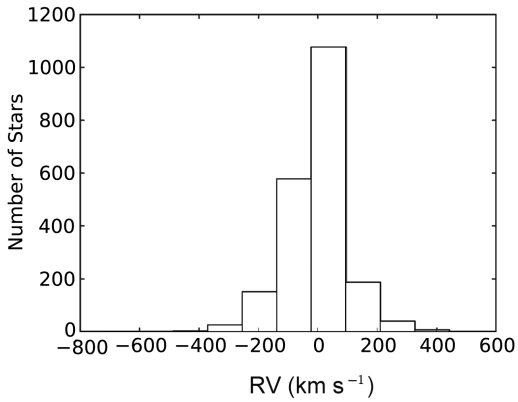

Fig. 4 Histogram of radial velocities for stars whose temperatures derived by SSPP have more than a 500 K difference with temperatures estimated by our method. These differences in temperature estimates cannot be due to radial velocity effects.

The Lick index measurement depends on the wavelength of the spectral features. These are sensitive to the star's radial velocity (RV) through the Doppler Effect. Hence, the accuracy of the temperature estimate may be affected by RV effects. However, Lick indices are originally defined on a lower resolution spectrum with no flux calibration. The spectral range of the index definition is broader than the real range encompassed by the spectral lines. That means a $small$ radial velocity will not affect the values of the Lick indices too much. To test this RV effect on the $T_{\rm eff}$ estimate, we have selected stars whose temperature from SDSS SSPP is more than 500 K off that given by our method.

Figure 4 shows the histogram of RV for these stars. With the peak of the RV distribution being close to zero, we may exclude RV effects from biasing our $T_{\rm eff}$ estimation method and being a cause for the observed systematic error.

4 CALIBRATION PROCESS

4.1 Model Spectra Selection for Stars

Once we have derived an estimate of the effective temperature of the target star using the Lick spectral index grid, we shall perform the calibration by 1) finding the best physical pseudo-continuum for the star, 2) finding the observed pseudo-continuum from the data and 3) dividing the latter by the former, with the quotient being the spectral response of the spectrograph.

The first step shall again use the Kurucz models in the following way. The Kurucz models use three parameters (effective temperature, $T_{\rm eff}$, surface gravity, $\log g$, and metallicity, [Fe/H]) to compute the emergent theoretical spectrum of the stellar atmosphere. Among these three parameters, the effective temperature plays a key role in the overall shape of the spectrum, especially the continuum.

Therefore, we have built an initial set of *combined models* by averaging all the models having the same effective temperature and various gravities and metallicities. For any $T_{\rm eff}$ found for a target star, we then derive the corresponding combined model by interpolating in the initial set of combined models. For $T_{\rm eff}$ higher than 9000 K we use the combined model at 9000 K and for $T_{\rm eff}$ lower than 3000 K we use the combined model at 3000 K.

4.2 Standard Stars for Each Spectrograph

After every exposure, there are up to 250 spectra on one given spectrograph. To perform the calibration, we must select some spectra as the standard or pseudo-standard stars in each spectrograph field. If genuine standard stars (for example, SDSS F8 subdwarf standards) are present with good quality spectra, they will be used. However, if genuine standard stars do not have good quality spectra or lack genuine standard stars, we are led to select stars which can become pseudo-standard ones using the Lick index grid method.

Before considering what kind of stars may be the best pseudo-standard stars, we need to analyze the errors of our method. How large the difference is between a star's actual $T_{\rm eff}$ and the Lick index grid estimate is not the most important factor. Let us consider two stars, of respective actual $T_{\rm eff}$ 6000 K and 8000 K, and let us suppose that our method gives respective estimates of 6200 K and 8500 K. The difference for the hotter star is larger than for the cooler. However, if the difference of the $model\ spectra$ between 8000 K and 8500 K is smaller than the difference of the $model\ spectra$ between 6000 K and 6200 K, we shall consider that the hotter star gives better accuracy than the cooler one and is therefore a more suitable pseudo-standard star candidate.

We thus may define what we call a Best Model Assessment Error, $\delta\_{\rm Model}$, as follows. In Figure 3, the cloud of representative points exhibits a dispersion around the solid line which is the best linear fit. After correction for the systematic error explained in Section 3 there remains a dispersion σ_T with an average value of 205 K. For a given $T_{\rm eff,grid}$ provided by the Lick index grid, we consider the two *combined* models of respective temperatures $T_1 = T_{\rm eff,grid} + \sigma_T$ and $T_2 = T_{\rm eff,grid} - \sigma_T$. We subsequently normalize the two extreme model fluxes by dividing their spectra by the average of their fluxes. The Best Model Assessment Error will be

$$\delta\_{\rm Model} = {\rm std}({\rm Combined\_Model}(T_1)_{\rm normalized} - {\rm Combined\_Model}(T_2)_{\rm normalized})\,, \quad (3)$$

where the combined model fluxes are considered across the spectral range 3800 Å to 9000 Å.

We have analyzed the 21 571 SDSS stellar spectra and computed the $\delta\_{\rm Model}$ for each. In Figure 5, this error is plotted versus temperature. Figure 5 shows that there is an optimum range of temperature where the Best Model Assessment Error is minimal, between 7200 K and 8000 K, which is still a useful range between 6000 K and 8000 K. The optimum roughly corresponds to average spectral types between F5 and A5, and these stars may be considered as the best pseudo-standard candidates for LAMOST's relative flux calibration based on our methodology. Note that

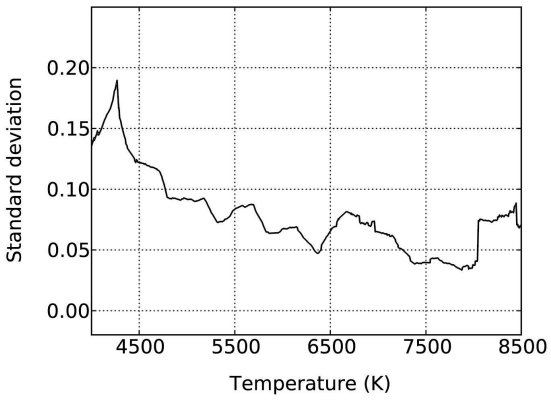

Fig. 5 Best Model Assessment Error (see definition in the text) versus effective temperature estimated by the Lick index grid on the 21 571 stars extracted from SDSS. The error has been normalized to the number of stars. The stars whose temperatures are in the range 7200 K–8000 K are suitable candidates for being pseudo-standard stars used in relative flux calibration.

the combined models cover all metallicities and gravities, while the SDSS spectrophotometric standards are selected as *metal poor F8 subdwarfs*: in fact, the systematically low metallicity of SDSS standards makes them have a higher average $T_{\rm eff}$ (because of weaker line blanketing) than the stars with normal metallicity from the same spectral type. Hence, our preferred pseudo-standard stars can be regarded as an extension of the more restricted SDSS standard sample.

4.3 Continuum Fitting and Response Function

To calculate the spectral response function of the spectrograph, pseudo-continua of both LAMOST spectra and model spectra are needed. When searching for the pseudo-continuum from the blue part or red part of LAMOST spectra, a simple polynomial function is not appropriate for real data fitting. Absorption features, especially extended molecular absorption bands, (e.g. CH, CN, C2, MgH in the blue, TiO in the red) and strong blends lead to underestimating the continuum. To solve this problem, we must first select parts of the spectrum not affected by these absorptions, then fit the set of selected regions with a continuous curve. Since an absorption band will locally influence the results of polynomial fitting, this influence will by itself be a good local absorption indicator. Let us first apply a median filter on a given spectrum; we get a flux density distribution A. Then, we use a polynomial of degree 7 to fit the spectrum (using least squares approximation and equal weight for all points): we get a smoothed flux density distribution B. Genuine pseudo-continuum ranges will be those where A and B distributions are closer. Any absorption band will separate B from A. Using this method, we select the best pseudo-continuum points and draw the trend of the spectrum. The method is illustrated in Figure 6.

The spectral response function of the spectrograph is then computed by Equation (4) on the selected pseudo-standard star spectra for each one. Further, this response function is applied to all other fiber spectra to calibrate them.

Normally, the spectral response function can be computed using flux standard stars. The common character of flux standard stars is that they have simple or even few lines. A or F type stars or white dwarfs are usually the candidates of flux standard stars. The formula for flux standard stars is similar to Equation (4) that replaces the $\mathrm{Continuum}_{\mathrm{LAMOST}}$ with $\mathrm{Continuum}_{\mathrm{flux\ standard\ star}}$. We compare the spectral response function computed by the method of this paper with that computed

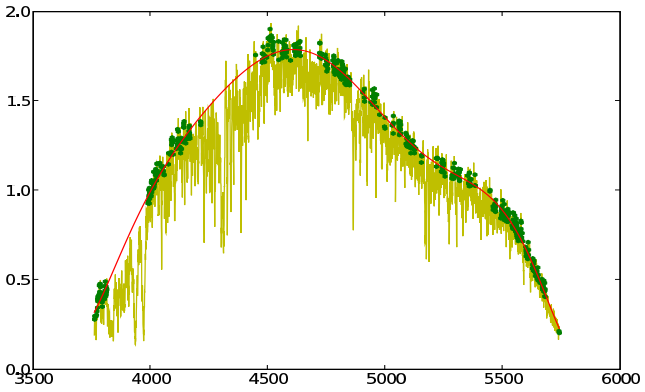

Fig. 6 The yellow line is the observed spectrum (*color online*). The green points are the points we have selected for describing the pseudo-continuum trend, comparing the median filter spectrum and the degree 7 polynomial filtered spectrum. The red line is the fitted pseudo-continuum. Wavelength is on the abscissa.

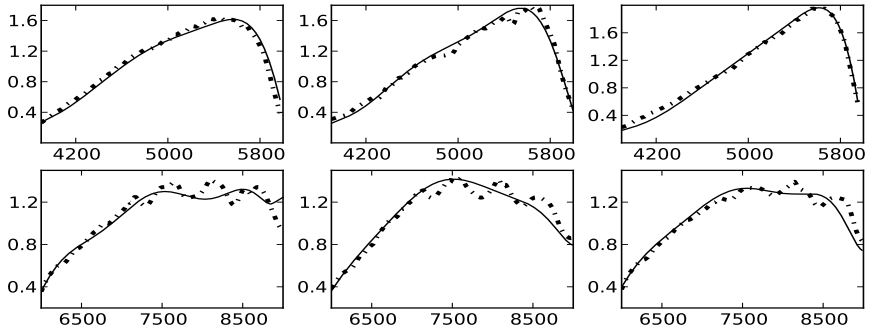

Fig. 7 Spectral Response Curves (SRC) are plotted in this figure. The x-axis is in Angstroms. The *solid lines* are computed by the method described in this paper. The *dashed lines* are computed by comparing the flux standard stars (selected by colors) with the Kurucz Model. *Top row*: blue arms of spectrographs 4 (*left*), 5 (*center*) and 13 (*right*); *Bottom row*: corresponding red arms of the above spectrographs.

by flux standard stars in Figure 7. The results show that the difference between the two spectral response functions is small.

$$\text{response function} = \frac{\text{Continuum}_{\text{LAMOST spectrum}}}{\text{Continuum}_{\text{model spectrum}}} . \tag{4}$$

5 TEST FOR THE METHOD

5.1 Observation and Data Reduction

We have tested this calibration method on a field observed by the LAMOST telescope during its commissioning phase between December 2010 and February 2011. All objects having spectra in

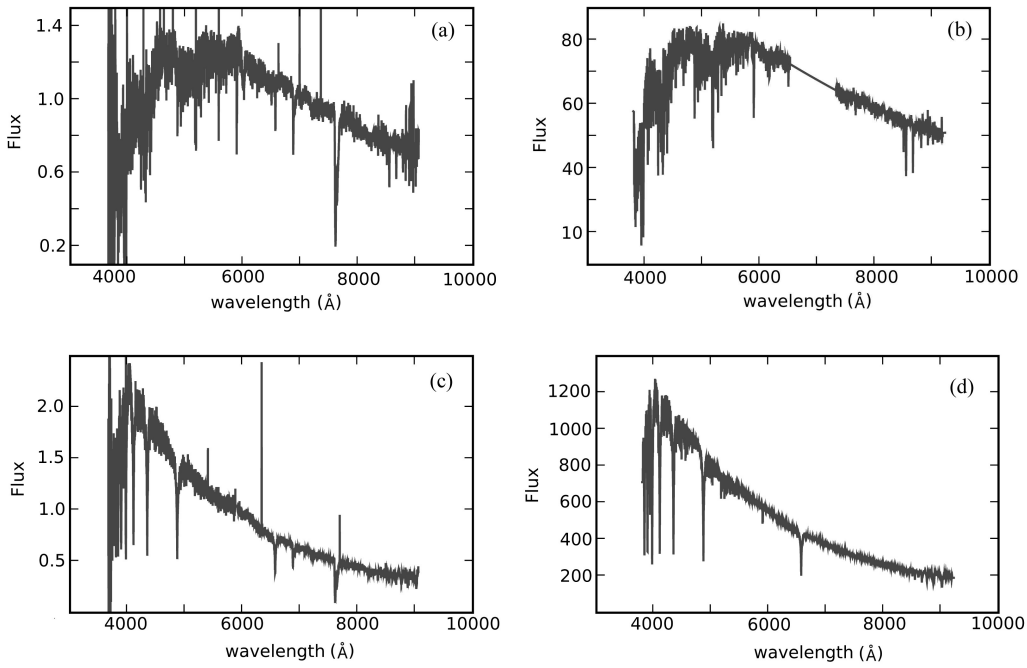

Fig. 8 (a) LAMOST spectrum of a star after relative calibration, (b) SDSS spectrum of the same target. The temperature of this star is 5313 K from SDSS SSPP. The same for a 8230 K star, (c): LAMOST and (d): SDSS.

the SDSS were picked out, and a signal to noise ratio of higher than 15 was further applied as an additional selection criterion. In total, we got a sample of 2000 spectra.

The original blue and red CCD frames were separately reduced by the basic LAMOST 2D data reduction pipeline. In the beginning, CCD biases are subtracted from the raw frames including arc lamp, twilight flat and scientific target ones. Each spectral frame includes 250 spectra and each spectrum covers about 16 pixels of fiber aperture. Twilight flat frames are used to trace the fiber spectra. One dimensional arc lamp, flat-field, sky, and target spectra are extracted using these traces and fiber aperture. Wavelength calibrations are performed with the help of the arc lamp and completed with sky emission lines which enforce calibration accuracy. Twilight flat frames are used to correct for differing individual fiber efficiencies (including detectors and spectrograph efficiencies, and possible vignetting), while blank night sky fibers are used to construct a super sky, which is interpolated to remove the sky light from the specified target spectra. Thus we get blue and red spectra with wavelength calibrations and sky subtractions.

The red spectrum has considerably strong atmospheric absorption lines from O2 and H2O around 6900 Å, 7200 Å, 7600 Å, and 8200 Å and an emission line at 6300 Å; the blue spectrum is affected by the strong 5577 Å [OI] atmospheric emission line, 5890 Å NaI and mercury vapor lines from city lights, but does not exhibit absorption bands. We mask the atmospheric absorption during the continuum fitting. All observed red spectra are corrected by this normalized spectrum.

Figures 8 and 9 display some examples of extracted spectra and fitted pseudo continua, and also the flux calibrated and combined spectra.

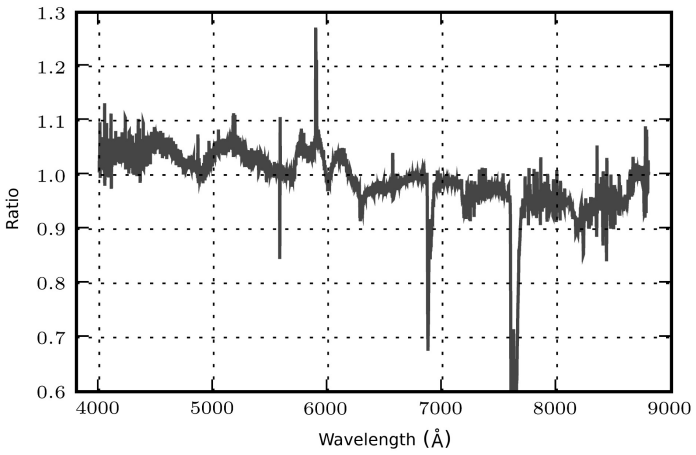

Fig. 9 Comparison between LAMOST spectra with our relative flux calibration and SDSS flux calibrated spectra on a preliminary common sample of 50 stars. On the ordinate, the mean value of the normalized flux ratio is obtained by dividing the LAMOST spectrum by the SDSS one. Excluding artifacts and dips coming from night sky emission lines, the mean ratio is consistently close to 1.0 across the whole spectral range.

5.2 Comparison with SDSS SPECTRA

To analyze the accuracy of the calibration, we selected stars observed by both LAMOST and SDSS. We have calibrated the LAMOST spectra and divided them by the spectra of the same sources from SDSS. The mean of the results is plotted in Figure 9 along the wavelength. Due to various reasons, this preliminary sample is restricted to only 50 stars in common to both instruments. The absorption lines near 6900 Å and 7600 Å are the oxygen and water vapor A band and B band of the Earth's atmosphere. The lines at 5577 Å and 5900 Å are the sky emission lines. Most of the other points are around 1.0, which means the accuracy of the calibration is above 90%.

6 CONCLUSIONS AND DISCUSSION

From the comparison with SDSS calibrated spectra, the accuracy of our relative calibration is good enough, and the effective temperature estimation is also reliable enough to pick out pseudo-standard stars. The more spectra in each sub field can be regarded as pseudo-standard stars, the better the accuracy of theoretical flux calibration will be. We need to do more experiments to study the statistical results of the number of standard stars and flux accuracy.

If we have photometric data for objects that have been relatively calibrated, absolute calibration could also be accomplished. However, the absolute calibration needs more careful investigation.

The success of calibration depends quite critically on the flat field. We are trying to develop a more robust flat field method. In this paper, twilight is used as the flat field, but twilight has its own gradients. Across each sub field of 1 degree, we ignored the variance of the sky, but in practice, it would be better to build a sky model for LAMOST. During commissioning, all calibrated data should be checked by eye.

Acknowledgements This work is funded by the National Natural Science Foundation of China (Grant No. 10973021). G. C. warmly thanks the Academy of Sciences of China for the grant of

a Visiting Professor for the senior International Scientist position at the National Astronomical Observatories of China in Beijing, and acknowledges the cheerful welcome by the LAMOST team.

This paper is based on public data of the Sloan Digital Sky Survey (SDSS). Funding for the SDSS and SDSS-II has been provided by the Alfred P. Sloan Foundation, the Participating Institutions, the National Science Foundation, the US Department of Energy, the National Aeronautics and Space Administration, the Japanese Monbukagakusho, the Max-Planck Society, and the Higher Education Funding Council for England. The Participating Institutions are listed at the official SDSS Web site, *http://www.sdss.org/*.

This paper makes use of data from the Sloan Digital Sky Survey.

References

Burstein, D., Faber, S. M., Gaskell, C. M., & Krumm, N. 1984, ApJ, 287, 586

Burstein, D., Faber, S. M., & Gonzalez, J. J. 1986, AJ, 91, 1130

Faber, S. M., Friel, E. D., Burstein, D., & Gaskell, C. M. 1985, ApJS, 57, 711

Gorgas, J., Faber, S. M., Burstein, D., et al. 1993, ApJS, 86, 153

Robinson, L. B., & Wampler, E. J. 1972, PASP, 84, 161

Su, D. Q., Cui, X., Wang, Y., & Yao, Z. 1998, in Society of Photo-Optical Instrumentation Engineers (SPIE) Conference Series 3352, ed. L. M. Stepp, 76

Sun, A., & Hu, J. 1997, Acta Astrophysica Sinica, 17, 213

Trager, S. C., Worthey, G., Faber, S. M., Burstein, D., & Gonzalez, J. J. 1998, ApJS, 116, 1

Worthey, G., Faber, S. M., Gonzalez, J. J., & Burstein, D. 1994, ApJS, 94, 687